ADVANCES IN ATMOSPHERIC SCIENCES, VOL. 36, JANUARY 2019, 55–64

• **Original Paper** •

Variation in Principal Modes of Midsummer Precipitation over Northeast China and Its Associated Atmospheric Circulation

Tingting HAN*[1,2], Shengping HE[1,3], Huijun WANG[1,2,4], and Xin HAO[1,2]

[1]*Collaborative Innovation Center on Forecast and Evaluation of Meteorological Disasters/Key Laboratory of Meteorological Disaster, Ministry of Education, Nanjing University for Information Science and Technology, Nanjing* 210044*, China*

[2]*Nansen-Zhu International Research Centre, Institute of Atmospheric Physics, Chinese Academy of Sciences, Beijing* 100029*, China*

[3]*Geophysical Institute, University of Bergen and Bjerknes Centre for Climate Research, Bergen* 5007*, Norway*

[4]*Climate Change Research Center, Chinese Academy of Sciences, Beijing* 100049*, China*

(Received 13 April 2018; revised 4 July 2018; accepted 12 July 2018)

ABSTRACT

This study documents the first two principal modes of interannual variability of midsummer precipitation over Northeast China (NEC) and their associated atmospheric circulation anomalies. It is shown that the first principal mode exhibits the largest amount of variability in precipitation over the south of NEC (referred to as the south mode), whereas the second principal mode behaves with the greatest precipitation anomaly over the north of NEC (referred to as the north mode). Further findings reveal that, through modulating moisture transportation and upper- and lower-troposphere divergence circulation as well as vertical movement over NEC, the anomalous northwestern Pacific anticyclone and the anticyclone centered over northern NEC exert the dominant influence on the south and north modes, respectively. Additionally, it is quantitatively estimated that water vapor across the southern boundary of NEC dominates the moisture budget for the south mode, while the north mode has a close connection with moisture through NEC's northern and western boundaries. Furthermore, the north (south) mode is strongly related to the intensity (meridional shift) of the East Asian westerly jet.

Key words: Northeast China, precipitation, northwestern Pacific anticyclone, Northeast China anticyclone

Citation: Han, T. T., S. P. He, H. J. Wang, and X. Hao, 2019: Variation in principal modes of midsummer precipitation over Northeast China and its associated atmospheric circulation. *Adv. Atmos. Sci.*, **36**(1), 55–64, https://doi.org/ 10.1007/s00376-018-8072-z.

1. Introduction

Northeast China (referred to as NEC hereafter), is composed of Heilongjiang Province, Jilin Province, Liaoning Province and the eastern four leagues of Inner Mongolia, and it is one of the regions most influenced by global warming in China (Zuo et al., 2004; Zhou et al., 2016). Climate change in this region, particularly the variation of precipitation, is of vital importance to grain yield, along with people's lives and social development. Precipitation in NEC mainly occurs during the summer, which is an important growing season for crops. Widespread precipitation anomalies generally induce extensive drought and flooding, causing great economic loss and casualties. Therefore, it is essential to explore the spatial and temporal characteristics of summer precipitation over NEC and its associated atmospheric circulations.

Summer precipitation over NEC is affected by the climate regimes over the northern middle and high latitudes, as well as tropical circulations, such as the Okhotsk high (Yao and Dong, 2000), the soil moisture in Northwest Eurasia (Zhu, 2011), the East Asian summer monsoon (Lian et al., 2003, Sun et al., 2017), the activity of cold vortices (Zhao and Sun, 2007; Hu et al., 2010), and the sea surface temperature (SST) in the tropical oceans (Feng et al., 2006; Gao and Gao, 2015). Sun et al. (2002) revealed that the East Asian trough, the subtropical high, the East Asian monsoon systems and the upper-level westerly jet all exert substantial impacts on drought and flooding in NEC during the summer. The Mongolian cyclone and the anticyclone south of Japan are also influential to midsummer precipitation over NEC (Jia and Wang, 2006). An abnormally strong cold vortex generally induces more precipitation and lower temperature anomalies over NEC during the summer (Feng et al., 2015; Li et al., 2015). The anomalous cold vortex activity is linked with the North Pacific oscillation (Liu et al., 2002), the northern hemispheric annual mode (He et al., 2006), and the blocking circulation over the Ural Mountains (Lian et al., 2010). As indicated by Wang and Ding (2009), the shifts and intensity of anomalous Asian polar vortex have an influence on the water vapor transport and precipitation amount over NEC. El Niño–Southern Oscillation is also considered to be a major con-

* Corresponding author: Tingting HAN
Email: hantt08@126.com

tributor to climatic change over NEC (Sun and Wang, 2006; Han et al., 2017). Additionally, the phase shifts of the Pacific Decadal Oscillation modulate the decadal variations of summer precipitation over NEC (Xu et al., 2015). The North Atlantic Oscillation (NAO) has an intensified influence on NEC precipitation during summer following the late 1970s (Sun and Wang, 2012), despite the weakened impact of the winter NAO on spring precipitation over southern China (Zhou, 2013). Wang and He (2015) determined that an anomalous Arctic sea-ice concentration excited intense Eurasian teleconnection and further affected the severe drought of 2014 over NEC. Recently, Han et al. (2018) noted that the early-spring SST anomalies in the tropical Indian Ocean have been a potential precursor of early-summer precipitation over NEC since the late 1980s.

The water vapor budget is closely associated with precipitation (Sun et al., 2011; Sun and Wang, 2013). Specifically, the transportation of moisture across the northern and southern boundaries exerts a great impact on summer precipitation over NEC (Gu et al., 2013). The net moisture input has decreased over NEC since the late 1990s, which directly caused a decadal reduction in summer precipitation in the region (Han et al., 2015). Wang et al. (2005) stated that only minimal amounts of water vapor originating from the Sea of Japan invade NEC during drought years, whereas the moisture derived from the East China Sea, the Yellow Sea and Inner Mongolia is transported to NEC during flood years. In addition, the three primary moisture passages contributing to heavy precipitation over NEC are the southeast transportation of moisture flow along the edge of the western Pacific subtropical high, the transportation of the southwest moisture current originating from the northern South China Sea, and the moisture transportation of the northwest stream that originates from westerly winds (Ma et al., 2017).

Furthermore, summer precipitation exhibits entanglement of spatial homogeneity and regional diversity over NEC. Although some efforts have been devoted to exploring the spatial characteristics through statistical classification, it is still unclear what the atmospheric circulation anomalies associated with the principal modes of summer precipitation over NEC are. In addition, the regimes influencing NEC precipitation are significantly different between early summer and midsummer (Shen et al., 2011). Midsummer is also a period of high concentration of precipitation for NEC. Thus, we discuss the principal modes of midsummer precipitation in NEC and their associated atmospheric circulation anomalies.

The rest of the paper is organized as follows: Section 2 describes the datasets and methods used in this study. Section 3 presents the principal modes of the interannual precipitation over NEC during midsummer and its associated atmospheric circulation anomalies. Conclusions are given in section 4.

2. Data and methods

The monthly atmospheric data used in this study are derived from the National Centers for Environmental Prediction–National Center for Atmospheric Research global atmospheric reanalysis dataset at a resolution of $2.5° \times 2.5°$ for 1948–2017 (Kalnay et al., 1996), including horizontal wind, vertical movement, specific humidity, and so on. The data of precipitation over China used in this study come from the monthly precipitation dataset from the National Climate Center of the China Meteorological Administration, collected for 160 stations, for the years 1951–2017. Another set of precipitation data used, on a $1.0° \times 1.0°$ latitude–longitude grid, is the Precipitation Reconstruction over Land (PREC/L) dataset from the National Oceanic and Atmospheric Administration for the years 1948–2017 (Chen et al., 2002). The time period of common overlap in the present study is from 1951 to 2017.

In this study, NEC is defined as the region north of 38°N and east of 119°E within the borders of China. Empirical orthogonal function (EOF) decomposition, and regression and correlation analyses are employed to explore the principal modes of midsummer precipitation over NEC and its associated atmospheric circulation anomalies. The precipitation over NEC is concentrated during July–August when the total percentage of precipitation is 49.1%. Thus, the midsummer mean in this study is calculated using the months of July and August. Additionally, the linear trends are removed prior to analysis to emphasize the interannual variability. The Student's *t*-test is used to detect the statistical significance of these analyses.

3. Results

3.1. *Principal modes of interannual precipitation over NEC during midsummer*

Figure 1 depicts the first two principal modes of midsummer precipitation over NEC, obtained from EOF analysis. These two principal modes explain 43.1% of the total variance. According to the method of North et al. (1982), the dominant mode of midsummer precipitation over NEC is well-separated from the second mode (figure not shown). The first principal mode (abbreviated as EOF1 hereafter) behaves homogenously over NEC, with the variability decreasing from south to north (Fig. 1a). The maximum variability of the EOF1 mode is located in the southern area of NEC. The EOF1 mode alone explains 31.3% of the total variance, indicating that it is the dominant midsummer precipitation mode in NEC. We further investigate the precipitation anomalies associated with the EOF1 mode using a regression of the PREC/L precipitation dataset on the time series for the first principal mode (referred to as PC1 hereafter). As shown in Fig. 1c, it is apparent that uniform changes in interannual precipitation appear over NEC during midsummer, and that the maximum anomaly prevails over the southern part of NEC. Therefore, the EOF1 mode is also designated as the south mode.

In contrast, the second principal mode (referred to as EOF2 hereafter) exhibits the greatest variability over the northern area of NEC (Fig. 1b), which explains 11.8% of the total variance. Figure 1d presents the linear regression pattern

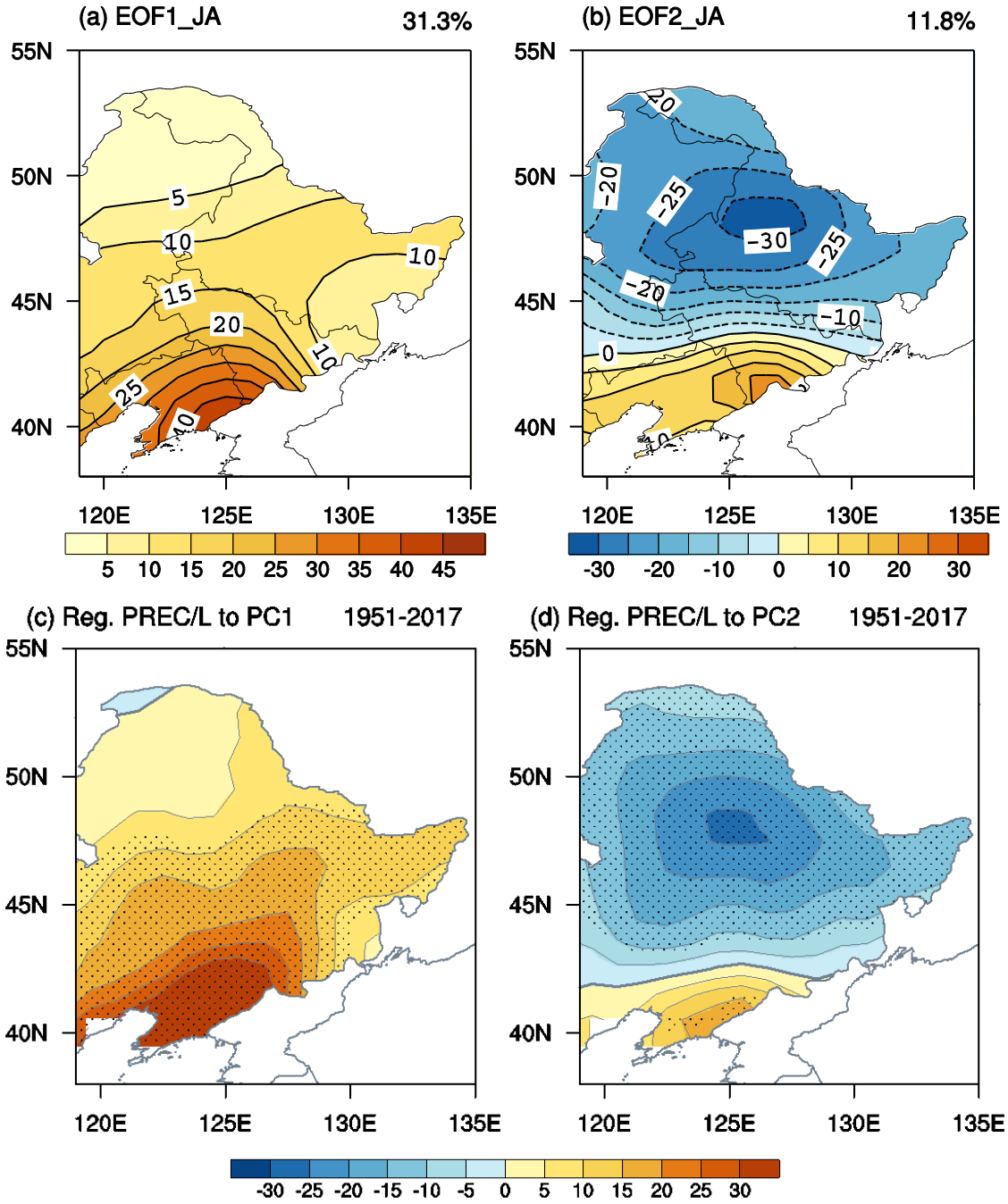

Fig. 1. The (a) first and (b) second principal modes for midsummer precipitation over NEC, determined by EOF analysis. The linear regression pattern of precipitation (units: mm) with regard to the time series for (c) PC1 and (d) PC2. Dotted areas are statistically significant at the 95% confidence level estimated using the Student's *t*-test.

of midsummer precipitation with regard to the time series of the second principal mode (referred to as PC2). It is evident that the greatest precipitation anomaly is positioned over the north of NEC. Consequently, the EOF2 mode is also designated as the north mode.

3.2. *Atmospheric circulation anomalies associated with the principal modes*

Different precipitation modes are attributed to different circulation anomalies. Figures 2a and b illustrate the horizontal wind anomalies at the lower troposphere associated with the two PCs. The south mode is characterized by significant anticyclonic wind anomalies over the northwestern Pacific, together with profound southwesterly wind anomalies over the area extending from eastern China to southern and eastern NEC. Easterly or southeasterly winds appear over the north of NEC. The southwesterly wind at the western flank of the anticyclone can drive warm wet air currents from the tropical West Pacific into eastern China, even extending farther northward towards NEC, particularly its southern parts. By

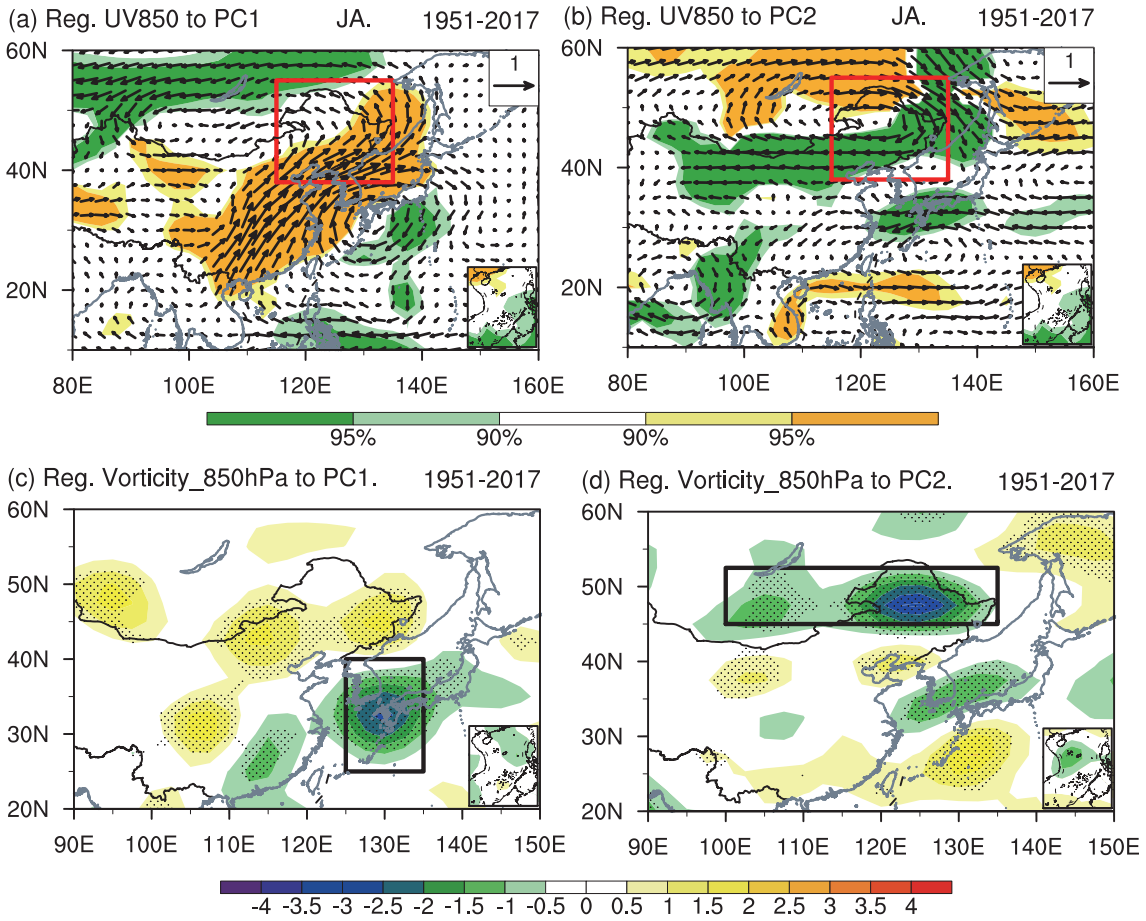

Fig. 2. Linear regression pattern of the midsummer horizontal wind at 850 hPa (UV850; units: m s^{-1}) against (a) PC1 and (b) PC2 during 1951–2017. Dark (light) shading indicates values that are statistically significant at the greater than 95% (90%) confidence level, estimated using the Student's *t*-test. (c, d) As in Figs. 1a and b but for the midsummer vorticity at 850 hPa (units: 10^{-6} s^{-1}). The red rectangles in (a) and (b) represent the NEC, and the black rectangles in (c) and (d) represent the selected regions for northwestern Pacific anticyclone index and northern NEC anticyclone index, respectively. Dotted areas indicate statistical significance at the 90% confidence level, estimated using the Student's *t*-test.

comparison, the north mode features a significantly anomalous anticyclonic wind field centered over northwestern NEC and an anomalous cyclonic wind field over the subtropical western Pacific. An anomalous westerly occupies the area north of 45°N within NEC, whereas an anomalous easterly occurs south of 45°N. The strong westerly transports water vapor and cold air from inland areas into NEC, especially into the north of NEC.

To facilitate our analysis, a northwestern Pacific anticyclone index (referred to as vorticiy_index1) is defined as the averaged vorticity within the region (25°–40°N, 125°–135°E) at 850 hPa (Fig. 2c). Another northern NEC anticyclone index (referred to as vorticity_index2) is calculated by averaging the vorticity within northern NEC (45°–52.5°N, 100°–135°E) at 850 hPa (Fig. 2d). These two anticyclone indices have been multiplied by −1 so that a positive index corresponds to strong anticyclone anomalies. The temporal evolutions of PC1 (solid line) and vorticity_index1 (dashed line) are shown in Fig. 3a. A significant covariability between the two indices can be observed during the period from 1951 to 2017, with a correlation coefficient of 0.51 (above the 99% confidence interval). Meanwhile, PC2 covaries closely with vorticity_index2 during the whole period of the study ($R = 0.61$; above the 99% confidence interval). This implies that the northwestern Pacific anticyclone anomaly and the anticyclone anomaly centered over northern NEC are important for the south and north modes of midsummer precipitation in NEC, respectively.

Furthermore, we examine the precipitation anomalies associated with the two anticyclone indices (Fig. 4). There are remarkably positive precipitation anomalies over NEC that are associated with a strong Northwest Pacific anticyclone. The maximum precipitation anomaly covers the southern part of NEC and is coincident with the south mode. However, when an anomalous anticyclone is centered over northern NEC, the largest precipitation anomaly is located over the northern portion of the region, in agreement with the north mode. These results confirm that the anticyclonic anomalies centered over the northwestern Pacific and over northern NEC are potential drivers for the first and second princi-

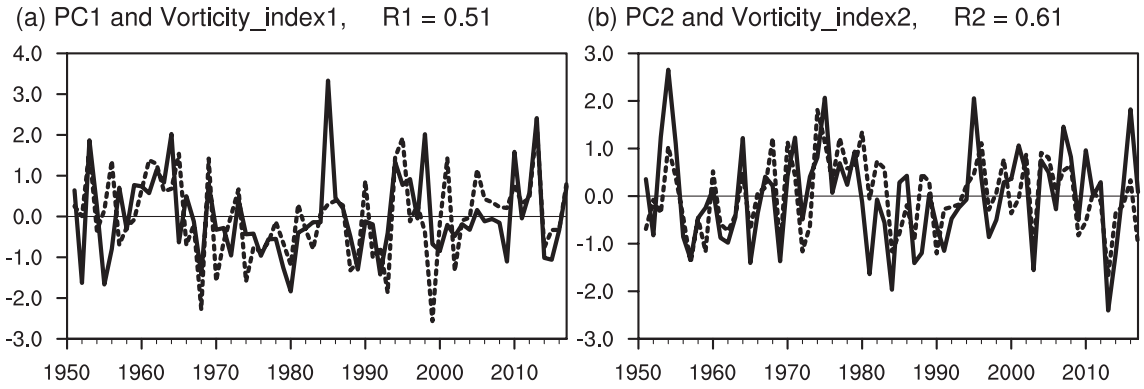

Fig. 3. (a) Time series of PC1 (solid line) and the northwestern Pacific anticyclone index (vorticity_index1; dashed line) for 1951–2017, both of which are normalized and detrended. (b) Time series of PC2 (solid line) and the northern NEC anticyclone index (vorticity_index2; dashed line) for 1951–2017, both of which are normalized and detrended.

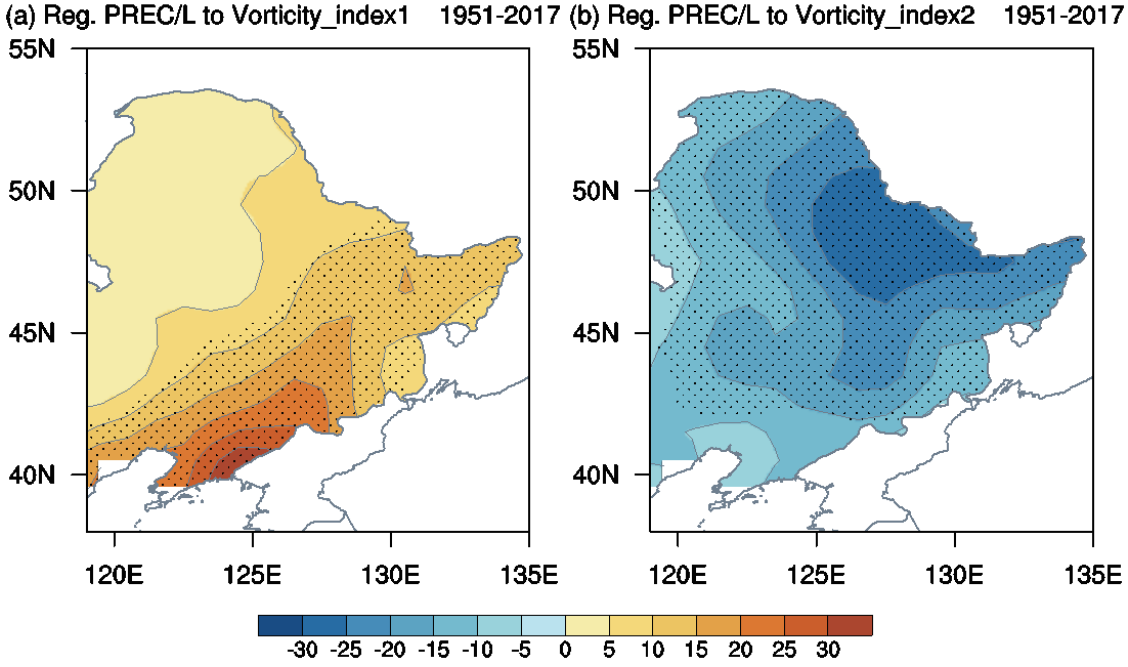

Fig. 4. Precipitation anomalies (units: mm) with regard to (a) vorticity_index1 and (b) vorticity_index2. Dotted areas are statistically significant at the 95% confidence level, estimated using the Student's *t*-test.

pal modes of the interannual precipitation, respectively, over NEC during midsummer.

To further illustrate the respective impacts of the anomalous anticyclones on the south and north patterns, the associated atmospheric circulation anomalies are explored in this section. Figures 5a and b present the linear regression of simultaneous horizontal wind at 850 hPa (UV850) against the two anticyclone indices. An anomalous anticyclone over the northwestern Pacific is accompanied by significant southwesterly winds over the area stretching from southern China to NEC, and the anomalous southerly winds transport warm and moist currents northward towards NEC. There exists a significant corresponding moisture divergence centered over the ocean as far south as the islands of Japan (Fig. 5c). The peripheral southwesterly flow conveys water vapor derived from the western Pacific and further invades NEC across its southern boundary. It is notable that a prominent convergence of moisture flux occurs over the south of NEC, which is favorable for the positive precipitation anomalies centering over southern NEC. Additionally, the water vapor flowing across the southern boundary makes a dominant contribution to the moisture input of that south pattern, with a correlation coefficient of 0.55 between the PC1 and the net moisture budget across the southern boundary (above the 99% confidence level). The net budgets of moisture across the western and eastern boundaries also exert an influence on the south mode, with respective correlation coefficients of 0.27 (above the 95% confidence level) and −0.37 (above the 99% confidence level) between PC1 and the net moisture budget through the western and eastern boundaries.

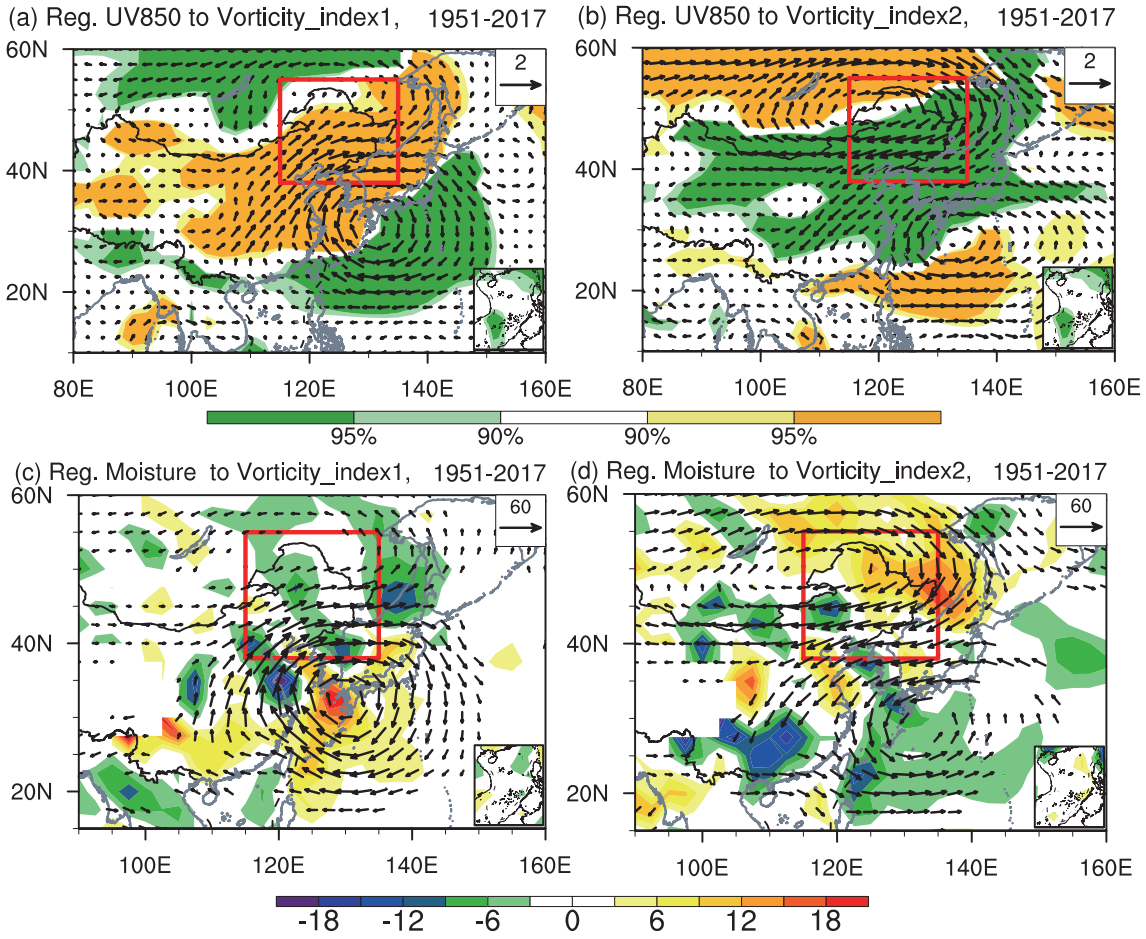

Fig. 5. Linear regression pattern of UV850 (units: m s^{-1}) during midsummer against (a) vorticity_index1 and (b) vorticity_index2 during 1951–2017. Dark (light) shading indicates values that are statistically significant at the greater than 95% (90%) confidence level, estimated using the Student's *t*-test. Linear regression pattern of the vertically integrated moisture flux against (c) vorticity_index1 and (d) vorticity_index2 during 1951–2017. The red rectangles represent the NEC. Vectors (units: kg m^{-1} s^{-1}) indicate the moisture flux that is statistically significant at the 90% confidence level, based on the Student's *t*-test. Shading (units: 10^{-6} kg m^{-2} s^{-1}) indicates moisture flux divergence anomalies associated with the two anticyclone indices.

Table 1. Correlation coefficients between the PCs and moisture incomes across the four boundaries of Northeast China during 1951–2017. Significant correlation coefficients at the 99% and 95% confidence levels are set in bold font with an asterisk and in regular font with an asterisk, respectively.

Correlation coefficients	Southern boundary	Northern boundary	Western boundary	Eastern boundary
PC1	**0.55***	−0.17	0.27*	**−0.37***
PC2	0.07	0.25*	−0.25*	−0.08

In association with an abnormal anticyclone centering over northern NEC, there are anomalous westerly or northwesterly winds visible over the north of NEC and anomalous easterly winds visible over the southern portion in the lower troposphere (Fig. 5b). The westerly or northwesterly anomalies determine the eastward transportation of water vapor and cold air from inland areas into NEC across the northern boundary (Fig. 5d). However, the water vapor is output from NEC by anomalous easterly or northeasterly winds through its western boundary. A significant corresponding moisture divergence anomaly is apparent over the north of NEC, and a convergence anomaly appears over the south. Specifically, the net moisture budgets across the northern and western boundaries have an intimate connection with the north mode, with a correlation coefficient of 0.25 and −0.25 between PC2 and the net moisture budgets across the northern and western boundaries, respectively (both above the 95% confidence level).

Figure 6 presents the linear regression of vertical movement against the two anticyclone indices. In response to an anomalous anticyclone over the northwestern Pacific, the anomalous convergence can be seen in the lower and middle troposphere and an anomalous divergence is also evident in the upper troposphere, exciting ascending motion over NEC. Such anomalous upward motion and abundant moisture content are conducive to the formation of a wet climate, especially over NEC's southern part (Figs. 4c and 5c). However,

the anticyclone centered over north NEC is concurrent with conspicuous divergent anomalies in the lower and middle troposphere, and convergent anomalies in the upper troposphere, inducing considerable descending movement. Interestingly, the anomalous divergence circulation is much stronger over the north of NEC than in the south, inducing stronger descending motion over the northern part than the southern part. This situation favors maximum negative anomalies of precipitation for the north mode (Fig. 4d).

Figure 7 displays the zonal wind anomalies in the upper troposphere related to the south and north patterns. The south mode is associated with significantly positive anomalies to the north of and negative anomalies to the south of the climatological East Asian westerly jet (EAJ), implying that the south mode may be linked with the meridional shift of the EAJ. Here, we define an EAJ displacement index as the difference between the zonal wind averaged within the region bound by (40°–50°N, 110°–140°E) and the region bound by (30°–40°N, 110°–140°E) at 250 hPa, which is similar to the methodology of Chen et al. (2016) but with the two averaging regions closer to NEC. The correlation coefficient of the EAJ displacement index with PC1 is 0.30, indicating that a positive/negative south pattern is associated with anomalously northward/southward shift of the EAJ. Chen et al. (2016) attributed the meridional shift of the EAJ to the anticyclonic/cyclonic anomaly over the Northwest Pacific.

The north mode corresponds to negative zonal wind anomalies along where the climatological EAJ lies (Fig. 7b). This suggests that the north mode may be associated with the intensity of the EAJ. We define an EAJ intensity index

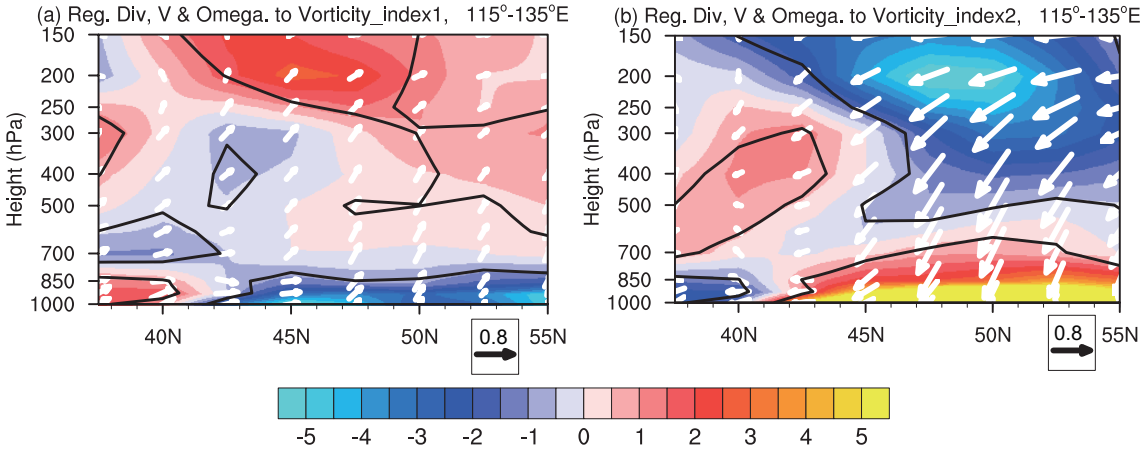

Fig. 6. Vertical–horizontal cross section averaged within (115°–135°E) for vertical wind (vectors; units: m s^{-1} and 10^{-2} Pa s^{-1}) and divergence (units: 10^{-7} s^{-1}) anomalies during the midsummer of 1951–2017 regressed onto (a) vorticity_index1 and (b) vorticity_index2. Divergence anomalies enclosed by black contours are statistically significant at the 90% confidence level, based on the Student's *t*-test.

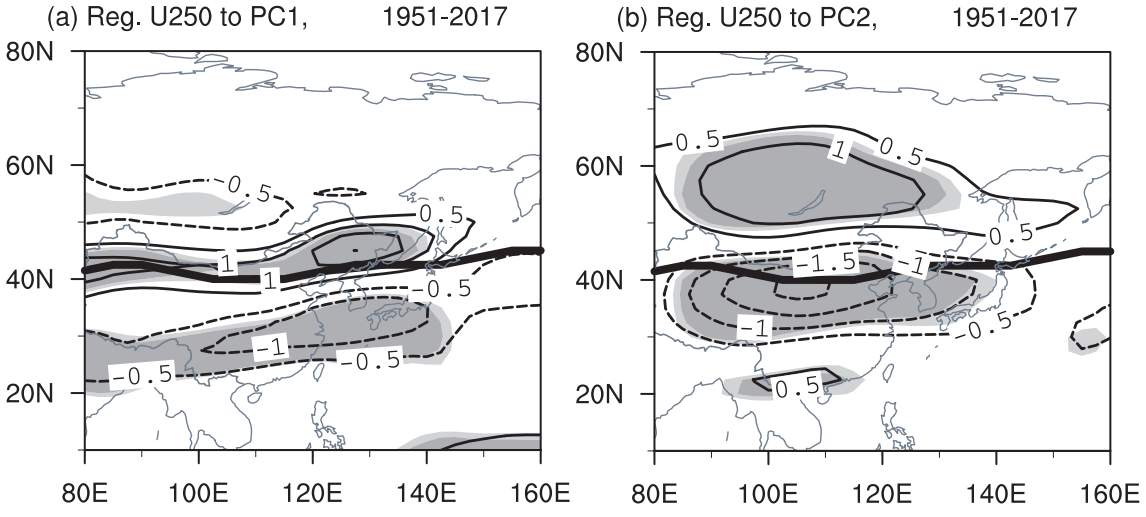

Fig. 7. Linear regression pattern of the zonal wind at 250 hPa (units: m s^{-1}) during midsummer of 1951–2017 regressed onto (a) PC1 and (b) PC2. Dark (light) shading indicates values that are statistically significant at the greater than 95% (90%) confidence level, estimated using the Student's *t*-test. The thick solid line represents the position of the climatological East Asian westerly jet.

by averaging the zonal wind within the region (35°–45°N, 110°–140°E), which is also similar to the approach of Chen et al. (2016) but with an averaging region nearer to NEC. The correlation coefficient of the EAJ intensity index and PC2 is −0.40, suggesting that a positive/negative north pattern is associated with a weakened/strengthened EAJ. The anomalous easterly at the southern flank of the anticyclone centered over northern NEC may account for the negative correlation between the EAJ intensity and the north mode (Fig. 2b).

4. Conclusions and discussion

This study investigates the first two principal modes of the interannual variability of precipitation in midsummer over NEC and their associated atmospheric circulation. The EOF1 presents the dominant variability over the south of NEC; that is, the south mode. This south mode is closely linked with the anticyclonic anomalies centered over the northwestern Pacific, with a correlation coefficient of 0.51 during the years 1951–2017. In response to an anomalous anticyclone over the northwestern Pacific, prominent southwesterly winds extend from eastern China to NEC, and an anomalous convergence of moisture occupies the southern part of NEC. The significant upper-level divergence anomalies and lower-level convergence anomalies excite strong vertical movement over NEC. These conditions are favorable for the formation of the south mode. Additionally, the dominant moisture income for the south mode is the water vapor coming across the southern boundary of NEC. The south mode is also associated with the meridional shift of the EAJ.

The EOF2 exhibits the dominant precipitation anomaly over the north of NEC; namely, the north mode. This pattern has a significant connection with the anomalous anticyclone centering over northern NEC, with a correlation coefficient of 0.61 during the years 1951–2017. The anomalous anticyclone centered over the northern NEC is accompanied by westerly anomalies over the north of NEC and easterly anomalies over the south, determining anomalous moisture divergence over the north of NEC and moisture convergence over the south. The anomalous upper-level convergence and lower-level divergence drive descending motion over NEC, with stronger anomalies over the northern portion than the southern portion of NEC. This situation favors maximum negative anomalies of precipitation for the north mode. In addition, the water vapor coming in through the northern and western boundaries dominates the net moisture income for the north mode. The intensity of the EAJ is also influential to the north mode.

The impact of tropical oceans on East Asian summer precipitation has been explored by many previous studies (Yuan et al., 2008; Han et al., 2017, 2018). For example, warming SST anomalies in the tropical Indian Ocean, especially in the northern Indian Ocean, lead to an anomalous anticyclone over the Northwest Pacific via a warming Kelvin wave anomaly and then induce precipitation anomalies over East China (Huang and Hu, 2008; Xie et al., 2009). Based on observations and numerical simulation, Yu et al. (2016) revealed that warming SST anomalies in the tropical Atlantic contributes to anomalous anticyclonic circulation over the Northwest Pacific through the Indian Ocean relaying effect. Additionally, SST anomalies in the equatorial central-eastern Pacific Ocean, in the Maritime Continent, and in the subtropical western North Pacific are also crucial to the interannual variability of the anticyclone over the Northwest Pacific during summer (He et al., 2015). Thus, the tropical oceans exert a great impact on the south mode of midsummer precipitation over NEC through modulating circulation anomalies over the Northwest Pacific. On the other hand, the anticyclone centered over NEC may be related to the atmospheric circulation anomalies at mid to high latitudes. Previous researches have shown that Arctic sea-ice cover and soil moisture in Eurasia are contributors to summer precipitation over NEC (Zhu, 2011; Han et al., 2015). Therefore, more efforts are required to explore the linkage between the north mode of the midsummer precipitation over NEC and the preceding Arctic sea-ice cover, snow cover and soil moisture in Eurasia.

Acknowledgements. We sincerely acknowledge the editor and two anonymous reviewers, whose kind and valuable comments greatly improved the quality of this manuscript. This work was jointly supported by the National Key Research and Development Program of China (Grant No. 2016YFA0600703), the National Natural Science Foundation of China (Grant No. 41805046), the Natural Science Foundation of the Jiangsu Higher Education Institutions of China (Grant No. 18KJB170013), the Startup Foundation for Introducing Talent of NUIST (Grant No. 2243141701085), and the funding of the Jiangsu Innovation and Entrepreneurship Team.

REFERENCES

Chen, M. Y., P. P. Xie, J. E. Janowiak, and P. A. Arkin, 2002: Global land precipitation: A 50-yr monthly analysis based on gauge observations. *Journal of Hydrometeorology*, **3**, 249–266, https://doi.org/10.1175/1525-7541(2002)003<0249:GLPAYM>2.0.CO;2.

Chen, W., and Coauthors, 2016: Variation in summer surface air temperature over Northeast Asia and its associated circulation anomalies. *Adv. Atmos. Sci.*, **33**, 1–9, https://doi.org/10.1007/s00376-015-5056-0.

Feng, G. L., and Coauthors, 2015: *Study on the Dynamical-Statistical Forecast of Precipitation During Flood Season in China*. Science Press, 250–252. (in Chinese)

Feng, X., X. Wang, and Y. Wang, 2006: Anomalies of the Northeast China floods season precipitation and SVD analysis with SSTA in world oceans. *Journal of Tropical Meteorology*, **22**, 367–373, https://doi.org/10.3969/j.issn.1004-4965.2006.04.008. (in Chinese with English abstract)

Gao, J., and H. Gao, 2015: Relationship between summer precipitation over northeastern China and sea surface temperature in the southeastern Pacific and the possible underlying mechanisms. *Chinese Journal of Atmospheric Sciences*, **39**, 967–977, https://doi.org/10.3878/j.issn.1006-9895.1503.14246. (in Chinese with English abstract)

Gu, Z. Q., Y. F. Gong, Q. Gong, L. Zhu, and H. Chao, 2013: The variation features of moisture budgets and its relationship

with precipitation over the Northeast area of China. *Journal of Chengdu University of Information Technology*, **28**, 651–658, https://doi.org/10.3969/j.issn.1671-1742. 2013.06.015. (in Chinese with English abstract)

Han, T. T., H. P. Chen, and H. J. Wang, 2015: Recent changes in summer precipitation in Northeast China and the background circulation. *International Journal of Climatology*, **35**, 4210–4219, https://doi.org/10.1002/joc.4280.

Han, T. T., H. J. Wang, and J. Q. Sun, 2017: Strengthened relationship between eastern ENSO and summer precipitation over Northeastern China. *J. Climate*, **30**, 4497–4512, https://doi.org/10.1175/JCLI-D-16-0551.1.

Han, T. T., S. P. He, X. Hao, and H. J. Wang, 2018: Recent interdecadal shift in the relationship between Northeast China's winter precipitation and the North Atlantic and Indian Oceans. *Climate Dyn.*, **50**, 1413–1424, https://doi.org/10.1007/s00382-017-3694-x.

He, C., T. J. Zhou., and B. Wu, 2015: The key oceanic regions responsible for the interannual variability of the western North Pacific subtropical high and associated mechanisms. *J. Meteor. Res.*, **29**, 562–575, https://doi.org/10.1007/s13351-015-5037-3.

He, J. H., Z. W. Wu, L. Qi, and A. J. Jiang, 2006: Relationships among the Northern Hemisphere annual mode, the Northeast cold vortex and the summer rainfall in Northeast China. *Journal of Meteorology and Environment*, **22**, 1–5 https://doi.org/10.3969/j.issn.1673-503X.2006.01.001. (in Chinese with English abstract)

Hu, K. X., R. Y. Lu, and D. H. Wang, 2010: Seasonal climatology of cut-off lows and associated precipitation patterns over Northeast China. *Meteor. Atmos. Phys.*, **106**, 37–48, https://doi.org/10.1007/s00703-009-0049-0.

Huang, G., and K. M. Hu, 2008: Impact of North Indian Ocean SSTA on Northwest Pacific lower layer anomalous anticyclone in summer. *Journal of Nanjing Institute of Meteorology*, **31**, 749–757, https://doi.org/10.3969/j.issn.1674-7097.2008.06.001. (in Chinese with English abstract)

Jia, X. L., and Q. Q. Wang, 2006: Analyses on general circulation character of precipitation anomaly in Northeast China flood season. *Plateau Meteorology*, **25**, 309–318, https://doi.org/10.3321/j.issn:1000-0534.2006.02.018. (in Chinese with English abstract)

Kalnay, E., and Coauthors, 1996: The NCEP/NCAR 40-year reanalysis project. *Bull. Amer. Meteor. Soc.*, **77**, 437–472, https://doi.org/10.1175/1520-0477(1996)077<0437:TNYRP>2.0.CO;2.

Li, W., X. Y. Shen, S. M. Fu, and W. L. Li, 2015: Quadrant-averaged structure and evolution mechanisms of a northeast cold vortex during its mature stage. *Atmospheric and Oceanic Science Letters*, **8**, 45–51, https://doi.org/10.3878/AOSL20140054.

Lian, Y., B. Z. Shen, Z. T. Gao, G. An, and X. L. Xiao, 2003: The study of the on-set criterion and the date of East Asian summer monsoon in Northeast China and its main characteristic analysis. *Acta Meteorologica Sinica*, **61**, 548–558, https://doi.org/10.11676/qxxb2003.055. (in Chinese with English abstract)

Lian, Y., C. Bueh, Z. W. Xie, B. Z. Shen, and S. F. Li, 2010: The anomalous cold vortex activity in Northeast China during the early summer and the low-frequency variability of the northern hemispheric atmosphere circulation. *Chinese Journal of Atmospheric Sciences*, **34**, 429–439, https://doi.org/10.3878/j.issn.1006-9895.2010.02.16. (in Chinese with English abstract)

Liu, Z. X., Y. Lian, Z. T. Gao, L. Sun, and B. Z. Shen, 2002: Analyses of the northern hemisphere circulation characters during northeast cold vortex persistence. *Chinese Journal of Atmospheric Sciences*, **26**, 361–372, https://doi.org/10.3878/j.issn.1006-9895.2002.03.07. (in Chinese with English abstract)

Ma, L. C., L. Sun, and N. Wang, 2017: Analysis of water vapor transport characteristics of typical rainstorm cases in Northeast China. *Plateau Meteorology*, **36**, 960–970, https://doi.org/10.7522/j.issn.1000-0534.2016.00078. (in Chinese with English abstract)

North, G. R., T. L. Bell, R. F. Cahalan, and F. J. Moeng, 1982: Sampling errors in the estimation of empirical orthogonal functions. *Mon. Wea. Rev.*, **110**, 699–706, https://doi.org/10.1175/1520-0493(1982)110<0699:SEITEO>2.0.CO;2.

Shen, B. Z., Z. D. Lin, R. Y. Lu, and Y. Lian, 2011: Circulation anomalies associated with interannual variation of early- and late-summer precipitation in Northeast China. *Science China Earth Science*, **54**, 1095–1104, https://doi.org/10.1007/s11430-011-4173-6.

Sun, B., and H. J. Wang, 2013: Water vapor transport paths and accumulation during widespread snowfall events in northeastern China. *J. Climate*, **26**, 4550–4566, https://doi.org/10.1175/JCLI-D-12-00300.1.

Sun, B., Y. L. Zhu, and H. J. Wang, 2011: The recent interdecadal and interannual variation of water vapor transport over Eastern China. *Adv. Atmos. Sci.*, **28**, 1039–1048, https://doi.org/10.1007/s00376-010-0093-1.

Sun, J. Q., and H. J. Wang, 2006: Regional difference of summer air temperature anomalies in Northeast China and its relationship to atmospheric general circulation and sea surface temperature. *Chinese Journal of Geophysics*, **49**, 662–671, https://doi.org/10.3321/j.issn:0001-5733.2006.03.008. (in Chinese with English abstract)

Sun, J. Q., and H. J. Wang, 2012: Changes of the connection between the summer North Atlantic Oscillation and the East Asian summer rainfall. *J. Geophys. Res.*, **117**, D08110, https://doi.org/10.1029/2012JD017482.

Sun, L., B. Z. Shen, B. Sui, and B. H. Huang, 2017: The influences of East Asian Monsoon on summer precipitation in Northeast China. *Climate Dyn.*, **48**, 1647–1659, https://doi.org/10.1007/s00382-016-3165-9.

Sun, L., G. An, Y. Lian, Z. T. Gao, X. L. Tang, B. Z. Shen, and L. Ding, 2002: The unusual characteristics of general circulation in drought and waterlogging years of Northeast China. *Climatic and Environmental Research*, **7**, 102–113, https://doi.org/10.3969/j.issn.1006-9585.2002.01.010. (in Chinese with English abstract)

Wang, H. J., and S. P. He, 2015: The North China/Northeastern Asia severe summer drought in 2014. *J. Climate*, **28**, 6667–6681, https://doi.org/10.1175/JCLI-D-15-0202.1.

Wang, X. Q., C. S. Chen, D. M. Shi, and Z. Y. Zhang, 2005: Anomaly water-vapor transportation of summer flood years in Northeast China. *Meteorology Monthly*, **31**, 44–47, https://doi.org/10.3969/j.issn.1000-0526.2005.09.009. (in Chinese with English abstract)

Wang, Z. Y., and Y. H. Ding, 2009: Impacts of the long-term change of the summer Asian polar vortex on the circulation system and the water vapor transport in East Asia. *Chinese Journal of Geophysics*, **52**, 20–29. (in Chinese with English abstract)

Xie, S. P., K. M. Hu., J. Hafner, H. Tokinaga, Y. Du, G. Huang, and T. Sampe, 2009: Indian Ocean capacitor effect on indo-western Pacific climate during the summer following El Niño. *J. Climate*, **22**, 730–747, https://doi.org/10.1175/2008JCLI2544.1.

Xu, Z. Q., K. Fan, and H. J. Wang, 2015: Decadal variation of summer precipitation over China and associated atmospheric circulation after the Late 1990s. *J. Climate*, **28**, 4086–4106, https://doi.org/10.1175/JCLI-D-14-00464.1.

Yao, X. P., and M. Dong, 2000: Research on the features of summer rainfall in Northeast China. *Quarterly Journal of Applied Meteorology*, **11**, 297–303, https://doi.org/10.3969/j.issn.1001-7313.2000.03.006. (in Chinese with English abstract)

Yu, J. H., T. Li, Z. M. Tan, and Z. W. Zhu, 2016: Effects of tropical North Atlantic SST on tropical cyclone genesis in the western North Pacific. *Climate Dyn*., **46**, 865–877, https://doi.org/10.1007/s00382-015-2618-x.

Yuan, Y., W. Zhou, J. C. L. Chan, and C. Y. Li, 2008: Impacts of the basin-wide Indian Ocean SSTA on the South China Sea summer monsoon onset. *International Journal of Climatology*, **28**, 1579–1587, https://doi.org/10.1002/joc.1671.

Zhao, S. X., and J. H. Sun, 2007: Study on cut-off low-pressure systems with floods over Northeast Asia. *Meteor. Atmos. Phys*., **96**, 159–180, https://doi.org/10.1007/s00703-006-0226-3.

Zhou, B. T., 2013: Weakening of winter North Atlantic oscillation signal in spring precipitation over southern China. *Atmospheric and Oceanic Science Letters*, **6**, 248–252, https://doi.org/10.3878/j.issn.1674-2834.13.0010.

Zhou, B. T., Y. Xu, J. Wu, S. Y. Dong, and Y. Shi, 2016: Changes in temperature and precipitation extreme indices over China: Analysis of a high-resolution grid dataset. *International Journal of Climatology*, **36**, 1051–1066, https://doi.org/10.1002/joc.4400.

Zhu, Y. L., 2011: A seasonal prediction model for the summer rainfall in Northeast China using the year-to-year increment approach. *Atmospheric and Oceanic Science Letters*, **4**, 146–150, https://doi.org/10.1080/16742834.2011.11446920.

Zuo, H. C., S. H. Lv, and Y. Q. Hu, 2004: Variations trend of yearly mean air temperature and precipitation in China in the last 50 years. *Plateau Meteorology*, **23**, 238–244, https://doi.org/10.3321/j.issn:1000-0534.2004.02.017. (in Chinese with English abstract)